Improving Simulation of a Tropical Cyclone Using Dynamical Initialization and Large-Scale Spectral Nudging: A Case Study of Typhoon Megi (2010)

WANG Hui[1,2] (王 慧), WANG Yuqing[2*] (王玉清), and XU Haiming[1] (徐海明)

1 *Key Laboratory of Meteorological Disaster of Ministry of Education, Nanjing University of Information Science & Technology, Nanjing* 210044, *China*

2 *International Pacific Research Center and Department of Meteorology, School of Ocean and Earth Science and Technology, University of Hawaii at Manoa, Honolulu, HI* 96822, *USA*

(Received November 21, 2012; in final form January 16, 2013)

ABSTRACT

In this study, an approach combining dynamical initialization and large-scale spectral nudging is proposed to achieve improved numerical simulations of tropical cyclones (TCs), including track, structure, intensity, and their changes, based on the Advanced Weather Research and Forecasting (ARW-WRF) model. The effectiveness of the approach has been demonstrated with a case study of Typhoon Megi (2010). The ARW-WRF model with the proposed approach realistically reproduced many aspects of Typhoon Megi in a 7-day-long simulation. In particular, the model simulated quite well not only the storm track and intensity changes but also the structure changes before, during, and after its landfall over the Luzon Island in the northern Philippines, as well as after it reentered the ocean over the South China Sea (SCS). The results from several sensitivity experiments demonstrate that the proposed approach is quite effective and ideal for achieving realistic simulations of real TCs, and thus is useful for understanding the TC inner-core dynamics, and structure and intensity changes.

Key words: dynamical initialization, large-scale spectral nudging

Citation: Wang Hui, Wang Yuqing, and Xu Haiming, 2013: Improving simulation of a tropical cyclone using dynamical initialization and large-scale spectral nudging: A case study of Typhoon Megi (2010). *Acta Meteor. Sinica*, **27**(4), 455–475, doi: 10.1007/s13351-013-0418-y.

1. Introduction

Significant progress has been made in high-resolution numerical simulations of tropical cyclones (TCs) since the pioneering work of Liu et al. (1997), who successfully simulated many aspects of Hurricane Andrew (1992) using a nested high-resolution model with explicit cloud microphysics. It is this realistic simulation that stimulated a series of studies that attempted to understand many aspects of TC inner core structure and dynamics (Liu et al., 1999; Zhang et al., 2000, 2001, 2002; Yau et al., 2004). These successful simulations also encouraged applications of nearly cloud-resolving dynamical prediction of TCs using nested high-resolution regional atmospheric models in various ocean basins (Davis et al., 2008; Hendricks et al., 2011; Tallapragada et al., 2012; Cha and Wang, 2013). Note that the global analysis fields are commonly used to provide both initial and lateral boundary conditions for limited-area models in numerical simulations of real TC cases, while the output from a global model prediction is used to drive a limited-area model in numerical prediction of TCs. Numerical simulations/predictions by a limited-area, high-resolution model are strongly constrained by the large-scale forcing through the lateral boundary condi-

Supported by the National Basic Research and Development (973) Program of China (2009CB421505), National Natural Science Foundation of China (41130964), and the United States NOAA/JHT grant (NA09OAR4310081). Additional support has been provided by the JAMSTEC, NASA, and NOAA through their sponsorships of the International Pacific Research Center (IPRC) in the School of Ocean and Earth Science and Technology (SOEST) at the University of Hawaii at Manoa.

*Corresponding author: yuqing@hawaii.edu.

tions. Since the analysis fields are closer to the actual atmospheric state than the global model prediction, a real case simulation is often more comparable with observations than a prediction. Therefore, a realistic simulation of a real TC case should not be mistaken as a skillful prediction. Nevertheless, a skillful prediction should not be expected if a model could not provide a successful simulation driven by good analysis fields. Because TCs always form over the open oceans where high temporal and spatial resolution in-situ observations are generally lacking, a realistic simulation can provide high-resolution datasets for process studies of real TCs, such as their genesis, rapid intensification, structure and intensity changes, island and terrain effects, and so on (e.g., Davis and Bosart, 2001, 2002; Braun, 2002, 2006; Wu et al., 2003, 2009; Zhu et al., 2004; Zhang et al., 2005; Braun et al., 2006; Cram et al., 2007; Musgrave et al., 2008; Yang et al., 2008; Hogsett and Zhang, 2009; Rogers, 2010; Hogsett and Zhang, 2010, 2011; van Nguyen and Chen, 2011; Yang et al., 2011; Zhang et al., 2011).

Sensitivity experiments perturbed from a realistic simulation are often used to isolate and understand individual dynamical/physical processes. For example, based on a real case simulation, Wu et al. (2003) investigated the eyewall evolution of Typhoon Zeb (1998) before, during, and after its landfall over the Luzon Island in northern Philippines. In a later study, Wu et al. (2009) further studied how the island landmass and the terrain over the land affected the eyewall evolution of Typhoon Zeb (1998) crossing Luzon Island, and they showed that the presence of Luzon Island plays a critical role in the observed eyewall evolution in Typhoon Zeb. In addition to the perturbed lower boundary forcing, sensitivity experiments with different physical parameterization schemes from the realistic control simulation are often used to understand the possible effects of various physical processes on a TC. For example, Braun and Tao (2000) and Li and Pu (2008) examined the sensitivity of the simulated TC intensity, rapid intensification, and boundary layer structure to the planetary boundary layer (PBL) parameterization scheme. Zhu and Zhang (2006) and Li and Pu (2008) studied the possible impact of cloud microphysical processes on the simulated TC structure, intensification, and the maximum intensity.

Although successful real-case simulations are very useful for process studies, to achieve realistic simulations of real-case TCs is often quite challenging. The difficulty stems from several key aspects, including the unrealistic representation of the initial TC intensity and structure and the bias in the simulated large-scale environmental flow field that governs the motion of the TC due to discrepancies in model physics and the predictability of the synoptic-scale atmospheric motion. In order to improve the initial TC structure and intensity in numerical simulations, various approaches have been proposed, such as implanting a bogus vortex, bogus data assimilation (BDA), dynamical initializations (DI), etc. The bogus vortex method is simply to use an analytical balance vortex to replace the weak vortex in the global (or regional) analysis at the initial time (Ueno, 1989; Leslie and Holland, 1995; Wang, 1998; Davis and Nam, 2001; Ma et al., 2007; Kwon and Cheong, 2010). Although this method is very easy to be implemented in any models, the three-dimensional structure of the TC is empirical and physical and dynamical inconsistencies often exist between the initial condition and the forecast model. The BDA method uses variational data assimilation with synthetic observations of the TC vortex that closely matches the observed TC intensity and structure (Goerss and Jeffries, 1994; Zou and Xiao, 2000; Pu and Braun, 2001; Zhang et al., 2007). Although this method can alleviate the possible inconsistencies between the initial field and the forecast model suffered by the direct bogus vortex scheme, its performance depends greatly on the availability of data in the observed TC. In most situations, bogus data based on some loosely constrained TC parameters are artificially specified. The DI is to achieve the TC initialization by integrating the forecast model (Bender et al., 1993; Kurihara et al., 1993; Peng et al., 1993; van Nguyen and Chen, 2011; Cha and Wang, 2013). This method has the advantage that the initial TC vortex is generated by the forecast model so that the initial TC vortex is dynamically and physically consistent with the forecast model.

There are several ways to generate the TC vortex by the DI method. Kurihara et al. (1993) spun up the axisymmetric component of the TC vortex by running the axisymmetric version of the forecast model while they constructed the asymmetric component by integrating a nondivergent barotropic model on a beta-plane using the initial conditions from the spun-up symmetric TC vortex. A similar DI scheme is used in the Navy regional coupled model for TC prediction (Hendricks et al., 2011), but the initial TC vortex is spun up in a three-dimensional TC model of Wang (2001) under idealized conditions. van Nguyen and Chen (2011) developed a DI scheme where a TC vortex is spun up through 1-h cycle runs from the initial forecast time. The initial condition generated by this DI scheme is dynamically consistent with the forecast model since the identical model is used in both the cycle runs and the forecast run. A similar DI scheme has been recently developed by Cha and Wang (2013) for real-time TC forecast. In their scheme, the TC vortex is spun up through the 6-h cycle runs initialized at 6 h before the initial forecast time. The most important part of their DI scheme is the use of a large-scale spectral nudging technique during the cycle runs so that the large-scale information can be well restored during the cycle runs.

Since the large-scale environmental flow plays an important role in controlling the TC motion, it is critical for a limited-area model to keep the evolution of the large-scale flow as close to the observation as possible. One way to do this is the scale-selective data assimilation using a three-dimensional variational (3DVAR) technique recently proposed by Liu and Xie (2012). By this approach, the large-scale information from a global forecast model is retained in a regional forecast model. Another way to keep the large-scale information of the driving field in a limited-area model is through the large-scale spectral nudging (SN) technique originally applied to dynamical downscaling using a regional model (von Storch et al., 2000; Feser and von Storch, 2008). This technique has recently been used in the cycle runs of the DI scheme for real-time dynamical TC forecasts by Cha and Wang (2013).

In this study, the cycle run DI scheme is combined with the large-scale SN to improve both the initial conditions of the TC structure and intensity and the simulation of a TC using the Advanced Weather Research and Forecasting (ARW-WRF) model. We will show that this combination is ideal for achieving realistic simulation of any TC if a high quality analysis and a good regional forecast model are available. The main objective of this paper is to demonstrate the effectiveness of the method using Typhoon Megi (2010) as an example. The method is briefly described in Section 2. The Typhoon Megi case is briefly discussed in Section 3 together with a description of the model setup and experimental design. Section 4 discusses the simulation results and demonstrates the effectiveness of the method in achieving an improved simulation of Typhoon Megi. A summary is presented in the last section.

2. Methodology

The DI scheme that we used to spin up the initial TC vortex includes two steps: vortex separation and cycle runs with SN. The core of the DI scheme is to spin up the axisymmetric TC vortex from the 3-h forward model integration with the use of the large-scale SN. Note that we use 3-h forward integrations (cycle runs) instead of 1-h integrations used in van Nguyen and Chen (2011). This allows the TC vortex to better adapt to the environment and to achieve the dynamical balance more sufficiently. To keep the environmental information as close to the observations as possible during the cycle runs, the SN scheme is used to retain motions with wavelengths longer than 1000 km. The approach was developed based on the ARW-WRF model, which includes three nested domains. The DI scheme is applied to both the outermost and the second domains because the innermost domain is not large enough to cover the major portion of the TC vortex. The SN scheme is only applied to the outermost domain which provides the lateral boundary conditions to the nested domains. The SN is applied not only to the cycle runs but also to the model simulation (see schematic diagram shown in Fig. 1).

2.1 Vortex separation

Since both the intensity and structure of a TC

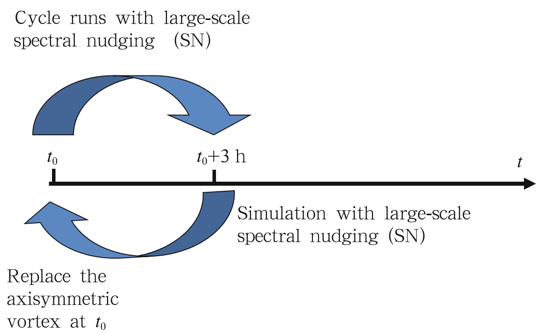

Fig. 1. Schematic diagram showing the flowchart of the dynamical initialization (DI) of the axisymmetric tropical cyclone (TC) vortex and the subsequent numerical simulation from t_0, both with the large-scale spectral nudging.

vortex in the global coarse-resolution analysis field are often unrealistic and the TC center may also deviate from that observed, the main objective of the DI scheme is to replace the unrealistic TC vortex by a more realistic and dynamically constrained TC vortex. Therefore, the first step of the DI is to separate the TC vortex from the total field of the global analysis. Here the vortex separation algorithm developed by Kurihara et al. (1993) and later modified by van Nguyen and Chen (2011) is utilized. The total field F in the global analysis (or model output) is first decomposed into the basic field ($F^{\rm b}$) and the disturbance field ($F^{\rm d}$). $F^{\rm b}$ is obtained by two sequential smoothing operations in zonal and meridional directions given below

$$\overline{F}^{\rm b}_{i,j} = F_{i,j} + K_m(F_{i-q_n,j} + F_{i+q_n,j} - 2F_{i,j}), \qquad (1)$$

$$F^{\rm b}_{i,j} = \overline{F}^{\rm b}_{i,j} + K_m(\overline{F}^{\rm b}_{i,j-q_n} + \overline{F}^{\rm b}_{i,j+q_n} - 2\overline{F}^{\rm b}_{i,j}), \qquad (2)$$

where F can be any scalar variable, such as sea level pressure, geopotential height, zonal and meridional winds, temperature, and water vapor mixing ratio; $q_n = \left[\frac{111\cos(\varphi_0)}{\Delta}\right]$ and $K_m = \left[\frac{1}{2}\left(1-\cos\frac{2\pi}{m}\right)\right]$, m = 2, 3, 4, 2, 5, 6, 7, 2, 8, 9, and 2; q_n is introduced in van Nguyen and Chen (2011) to make the filtering algorithm more applicable to any horizontal grid spacing Δ less than 100 km, φ_0 is the latitude of the observed TC center, [ ] denotes the nearest integer grid index, and i, j are the grid point indices in zonal and meridional directions. By application of this filtering operation, all components with horizontal wavelengths less than 900 km are completely removed, namely, the inner core part of the TC vortex in the analysis field is totally removed. The disturbance field is then easily obtained as the residual by subtracting the basic field from the original total field, namely, $F^{\rm d} = F - F^{\rm b}$, no matter for the analysis data or for the model output.

The disturbance field ($F^{\rm d}$) contains not only the TC vortex ($F^{\rm hv}$) but also the non-TC perturbation ($F^{\rm n-hv}$). Following Kurihara et al. (1993), we use the cylindrical filter centered at the TC center in the analysis field or model output to isolate the TC vortex from the disturbance field as given below

$$F^{\rm hv}(r,\theta) = F^{\rm d}(r,\theta) - \{F^{\rm d}(r_0,\theta)E(r) + \overline{F^{\rm d}}(r_0)[1-E(r)]\}, \qquad (3)$$

where $E(r) = \dfrac{\exp[-(r_0-r)^2/l^2] - \exp[-\frac{(r_0)^2}{l^2}]}{1-\exp[-\frac{(r_0)^2}{l^2}]}$, r is the radius from the TC center and θ is the azimuth, and r_0 is the radius out of which the TC component becomes zero, which is set to be 600 km here (theoretically it should be adjusted according to the size of the targeted TC vortex). The weighting function $E(r)$ smoothly changes with radius from 0 at $r = 0$ to 1 at $r = r_0$. In $E(r)$, l is a parameter controlling the filter shape and is set to be 1/5 of r_0 as in Kurihara et al. (1993).

The asymmetric part of the TC component is known to play an important role in controlling TC motion (Holland, 1983; Kurihara et al., 1993, 1995). We simply assume that the asymmetric part is reasonably resolved in the analysis field although the axisymmetric flow in the inner core region is substantially weak compared to the actual TC. Therefore, in the DI scheme, the TC vortex field is further decomposed into the axisymmetric ($F^{\rm ax} = \frac{1}{2\pi}\oint F^{\rm hv}{\rm d}\theta$) and asymmetric ($F^{\rm as} = F^{\rm hv} - F^{\rm ax}$) components. In the cycle runs described below, only the axisymmetric TC component is spun up while the basic field, the asymmetric TC component, and the non-TC perturbation field remain unchanged.

2.2 Cycle runs and vortex construction

The cycle run is the key of the DI scheme. It spins up the axisymmetric TC vortex component as done recently in Cha and Wang (2013). Each cycle run is initialized at the initial model simulation time t_0 and is integrated for 3 h. In the first cycle run, the axisymmetric TC vortex in the analysis field is relocated to the observed TC center if the center of the vortex in the analysis field is deviated from that observed. In all the subsequent cycle runs, the axisymmetric TC vortex from the current cycle run is used to replace the axisymmetric vortex in the previous cycle run at t_0. The cycle run is repeated until the intensity of the TC vortex from the last cycle run is comparable to the observed TC intensity. To ensure a smooth merging of the axisymmetric TC vortex from the cycle run and the rest of the field at t_0, we define $F^{\mathrm{ax}}_{t=0}$ and $F^{\mathrm{ax}}_{t=3}$ as the axisymmetric TC vortex both at the initial time t_0 and after a cycle run, and construct a new axisymmetric TC vortex by

$$F^{\mathrm{ax}}_{\mathrm{new}} = wF^{\mathrm{ax}}_{t=0} + (1-w)F^{\mathrm{ax}}_{t=3}, \tag{4}$$

where w is a weighting function given below

$$w = \begin{cases} 0.0 & r > \dfrac{r_0}{2}, \\ 0.5\left[1+\cos 2\pi\left(\dfrac{r-r_0}{r_0}\right)\right] & \dfrac{r_0}{2} \leqslant r \leqslant r_0, \\ 1.0 & r > r_0. \end{cases} \tag{5}$$

From Eqs. (4) and (5), we can see that the inner part ($r < r_0/2$) of the axisymmetric TC component is replaced by the axisymmetric component from the 3-h cycle run, while the outer region ($r > r_0 = 600$ km) is determined by the axisymmetric component in the original analysis field. This implicitly assumes that the storm-scale outer circulation can be reasonably resolved by the global analysis. Therefore, the DI scheme through the cycle runs only enhances the axisymmetric TC core where the global analysis could not resolve. The new axisymmetric vortex given in Eq. (4) is merged with the other components defined earlier to form the initial field for the next cycle run.

2.3 Spectral nudging

The SN technique has been widely used in regional climate modeling (e.g., Kida et al., 1991; von Storch et al., 2000; Riette and Caya, 2002; Miguez-Macho et al., 2005; Cha et al., 2011). It allows the model to nudge only the selected component in a model simulation. For example, in most applications, the large-scale component or the driving field in a limited-area model is expected to remain close to the observation. Such a large-scale nudging can be mathematically expressed as

$$\frac{\partial Q}{\partial t} = F(Q) + \alpha(Q^{\mathrm{L}}_{\mathrm{G}} - Q^{\mathrm{L}}_{\mathrm{R}}), \tag{6}$$

where Q is a model prognostic variable, F is the model operator, α (= 0.0003, corresponding to an e-folding damping time of 55.6 min) is a nudging coefficient, and $Q^{\mathrm{L}}_{\mathrm{G}}$ and $Q^{\mathrm{L}}_{\mathrm{R}}$ are the large-scale components of the global analysis and the model forecast, respectively. From Eq. (6), we can see that the large-scale SN constrains the model simulated large-scale component close to the global analysis at any given time during the model integration. Therefore, the application of the large-scale SN can prevent the large-scale component in the regional model integration from drifting from the driving field.

The SN is a new option for the upper-air nudging since the ARW-WRF version 3.1. Currently the SN can be applied to zonal and meridional wind components, potential temperature, and water vapor mixing ratio in the ARW-WRF model. In a recent study, Cha and Wang (2013) used the large-scale SN in the outmost model domain in their DI scheme to reduce errors in the large-scale motion during the cycle runs. They nudged both the large-scale wind and temperature fields in the mid-upper troposphere. In our application, the SN is applied only to the mid-upper tropospheric wind field in the outermost domain. Note that since our interest is to achieve realistic simulation, not prediction, of the TC motion, structure and intensity changes, we use the SN to preserve the large-scale wind field with wavelengths longer than 1000 km not only during the cycle runs in the DI scheme but also throughout the model simulation as discussed in the following two sections.

3. Typhoon Megi (2010), model settings, and experimental design

3.1 An overview of Typhoon Megi (2010)

Typhoon Megi (2010) was the most powerful and longest lived TC over the western North Pacific

(WNP) and South China Sea (SCS) in 2010. It was first identified as a tropical disturbance by the Joint Typhoon Warning Center (JTWC) on 12 October. The Japan Meteorological Agency (JMA) and JTWC began to monitor the low-level cyclonic circulation as a tropical depression (TD). The TD further intensified into a tropical storm (TS), named Megi by JMA at 1200 UTC 12 October. Later, on 14 October, an eye of the storm could be clearly seen from satellite images, and thus JMA upgraded Megi to a severe tropical storm (STS) and JTWC upgraded it to a category-1 typhoon. JMA upgraded Megi to a typhoon on 15 October.

As shown in Fig. 2, Megi initially moved northwestward and then turned west-southwestward. It experienced a rapid intensification from 16 to 18 October during which Megi attained its peak intensity with the central sea level pressure (SLP) of 905 hPa and the maximum 10-m wind speed of 80 m s^{-1}, the only super typhoon over the WNP in 2010. Megi made landfall over the Luzon Island in northern Philippines at around 0325 UTC 18 October. It weakened to a category-2 typhoon immediately after its landfall over the Luzon Island. After crossing the Luzon Island, Megi entered the SCS and turned northwestward and then suddenly northward. During its northward turning over the SCS, Megi slowed down while re-intensified from category-2 to category-4 with the central SLP of 935 hPa and the maximum 10-m sustained wind speed of 57 m s^{-1}. Early on 20 October, Megi turned north-northeastward. It then weakened to a TS, and finally a TD, and made its second landfall at Zhangpu in Fujian Province, China on 23 October and dissipated on the next day.

In addition to the distinct track and intensity changes (Fig. 2), Megi also experienced remarkable structure changes. For example, the storm size increased rapidly during its rapid intensification stage. Its original eyewall experienced a breakdown when it crossed the Luzon Island and redeveloped shortly after it entered the SCS. A new outer eyewall formed at a larger radius as a result of the axisymmetrization of outer spiral rainbands (Fig. 3). In the meantime, a new inner eyewall re-formed in the eye region of the large outer eyewall, a double eyewall phenomenon never being documented before.

3.2 Model settings

The numerical simulations of Typhoon Megi presented in this study were performed using the ARW-WRF model version 3.3.1. The model atmosphere is fully compressible and nonhydrostatic. The model uses the terrain-following, hydrostatic-pressure (σ) as the vertical coordinate. The model domain is two-way interactive, triply nested. The three meshes have sizes of 455×375, 436×436, and 328×328 grid points with horizontal grid spacings of 18, 6, and 2 km, respectively. The resolutions of the terrain height and land-

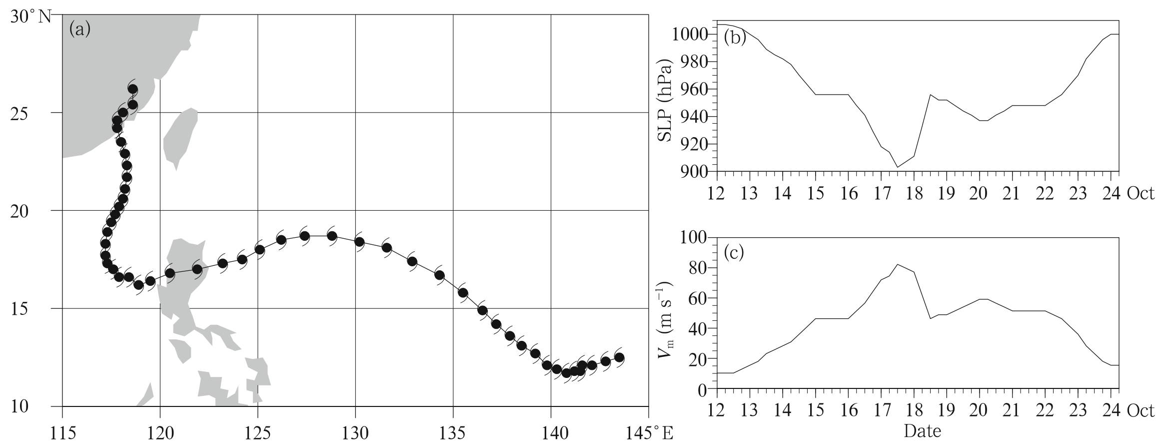

Fig. 2. (a) Track of Typhoon Megi (2010) at 6-h intervals, and the time series of (b) central sea level pressure (hPa) and (c) maximum sustained 10-m wind speed (m s^{-1}) of the JTWC best track data from 0000 UTC 12 to 0000 UTC 24 October 2010.

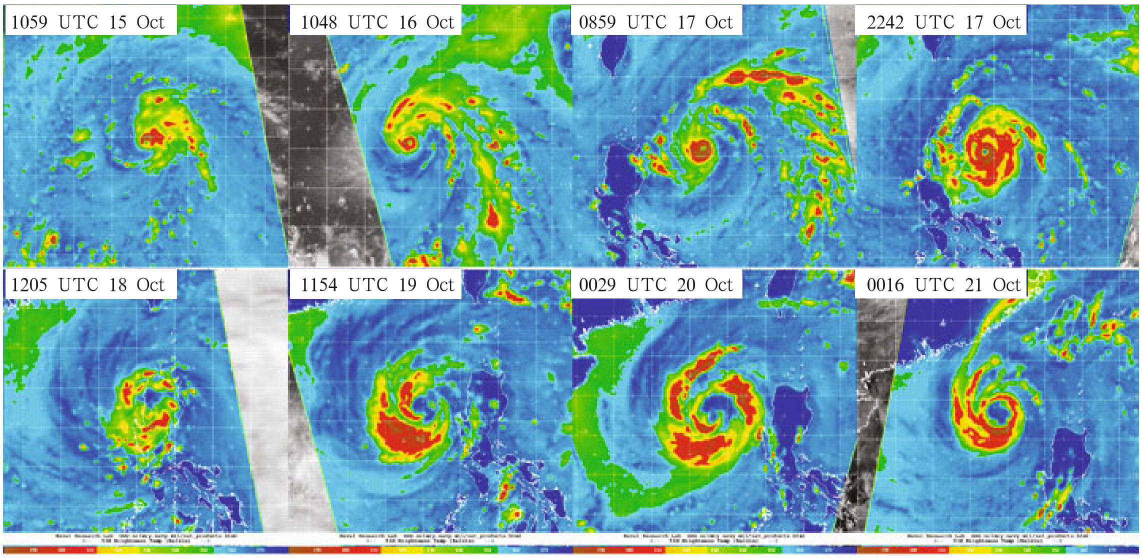

Fig. 3. Satellite images at given times during 15–21 October 2010, showing the inner core size increase before Typhoon Megi (2010) made landfall over the Luzon Island and the remarkable structure changes when the typhoon crossed the Luzon Island. Courtesy of the US Naval Research Lab.

use data for these meshes are 5 min, 2 min, and 30 s (about 9, 4, and 1 km), respectively. There are 36 uneven σ-levels for all meshes extending from the surface to the model top at 50 hPa. Both the 6- and 2-km meshes automatically move following the TC center during the simulation to allow the TC inner core to be covered in the nested meshes (Fig. 4). The outermost 18-km mesh is fixed during the model integration. Most of the results discussed below are the output from the innermost mesh. The model physics include (1) the single-moment 6-class cloud microphysics scheme (WSM6, Hong and Lim, 2006) for grid-scale moist processes; (2) the Mellor-Yamada Nakanishi and Niino level-2.5 turbulence closure scheme (Nakanishi and Niino, 2004) for subgrid-scale vertical mixing with the Monin-Obukhov similarity theory for surface flux calculations over the ocean where the roughness length for momentum is modified for TC strength winds (Moon et al., 2007); (3) the Rapid Radiative Transfer Model (RRTM) (Mlawer et al., 1997) for longwave radiation calculation and Dudhia scheme (Dudhia, 1989) for shortwave radiation calculation; (4) the NOAH land surface scheme (Ek et al., 2003) for land surface processes; and (5) the Kain-Fritsch cumulus parameterization scheme (Kain and Fritsch, 1990, 1993; Kain, 2004) for deep and shallow convection in the outermost domain. We assume that convection can be roughly resolved in the two inner nested meshes. Dissipative heating is considered in all model meshes.

The model initial and lateral boundary conditions for both cycle runs and model simulations are interpolated from the National Centers for Environment Prediction (NCEP) global final (FNL) analysis which has a horizontal resolution of $1^\circ \times 1^\circ$ on 27 uneven pressure levels. The daily sea surface temperature (SST) data-

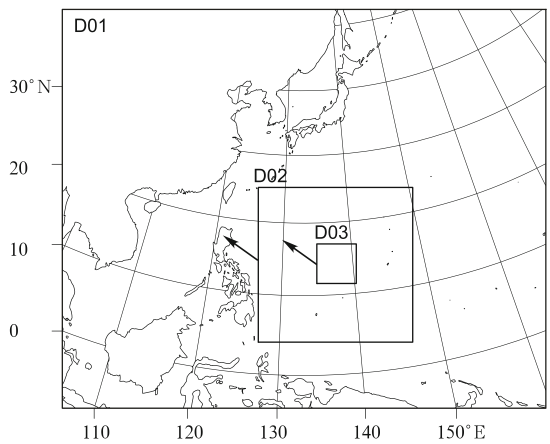

Fig. 4. The triply-nested, movable mesh model domains used for Typhoon Megi simulation in this study.

set at a 1°×1° resolution is also from the FNL. The details for the DI and the experimental design for Typhoon Megi (2010) are discussed below.

3.3 DI for Typhoon Megi

The DI scheme described in Section 2 was used to initialize Typhoon Megi at 0000 UTC 15 October 2010, which is about one day before the onset of rapid intensification (RI) of the storm. In the Megi case, after 5 cycle runs, the model TC obtained the intensity comparable to that observed in the JTWC best track data and achieved the structure typical of a strong TC. Figure 5 shows the SLP fields from the initial FNL analysis and those from the first, third, and fifth cycle runs, respectively. In the initial FNL analysis field, the central SLP of the TC vortex is too weak compared to that from the JTWC best track data (1002.1 versus 956 hPa), mainly because the storm core was not resolved well by the coarse resolution FNL analysis. The vortex deepened gradually after each cycle run and the TC vortex developed a compact inner core structure, consistent with observations (Fig. 3). After 5 cycle runs, the TC vortex reached an intensity with a central SLP of 956.4 hPa and the maximum 10-m sustained wind speed of 45.2 m s^{-1}, compared well with the observed 956 hPa and 45 m s^{-1} in the JTWC best track data.

In addition to the storm intensity, the DI also produced the realistic storm structure. As we can see from the azimuthal mean tangential wind given in Fig. 6,

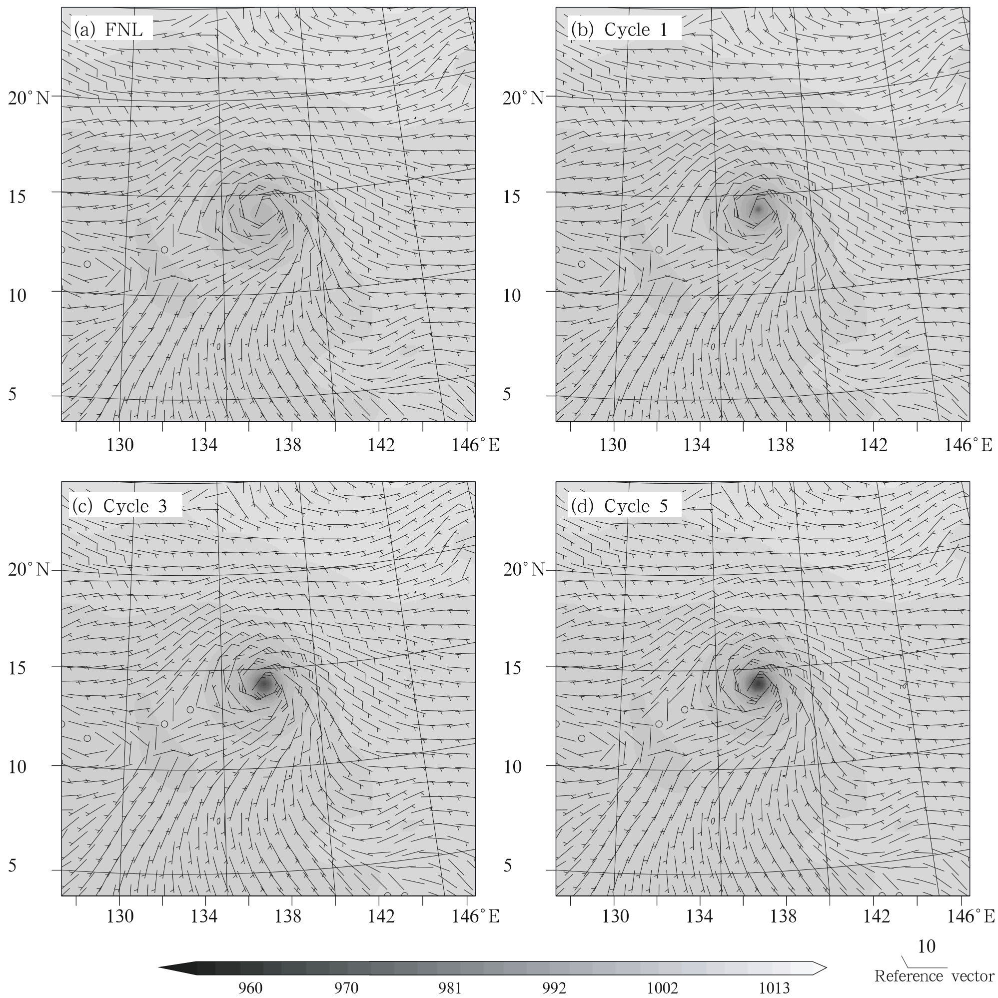

Fig. 5. The sea level pressure field (hPa; shaded) superimposed with the surface winds (wind bars) from (a) the NCEP FNL analysis; and from the dynamical initialization after (b) 1 cycle run, (c) 3 cycle runs, and (d) 5 cycle runs for Typhoon Megi at 0000 UTC 15 October 2010.

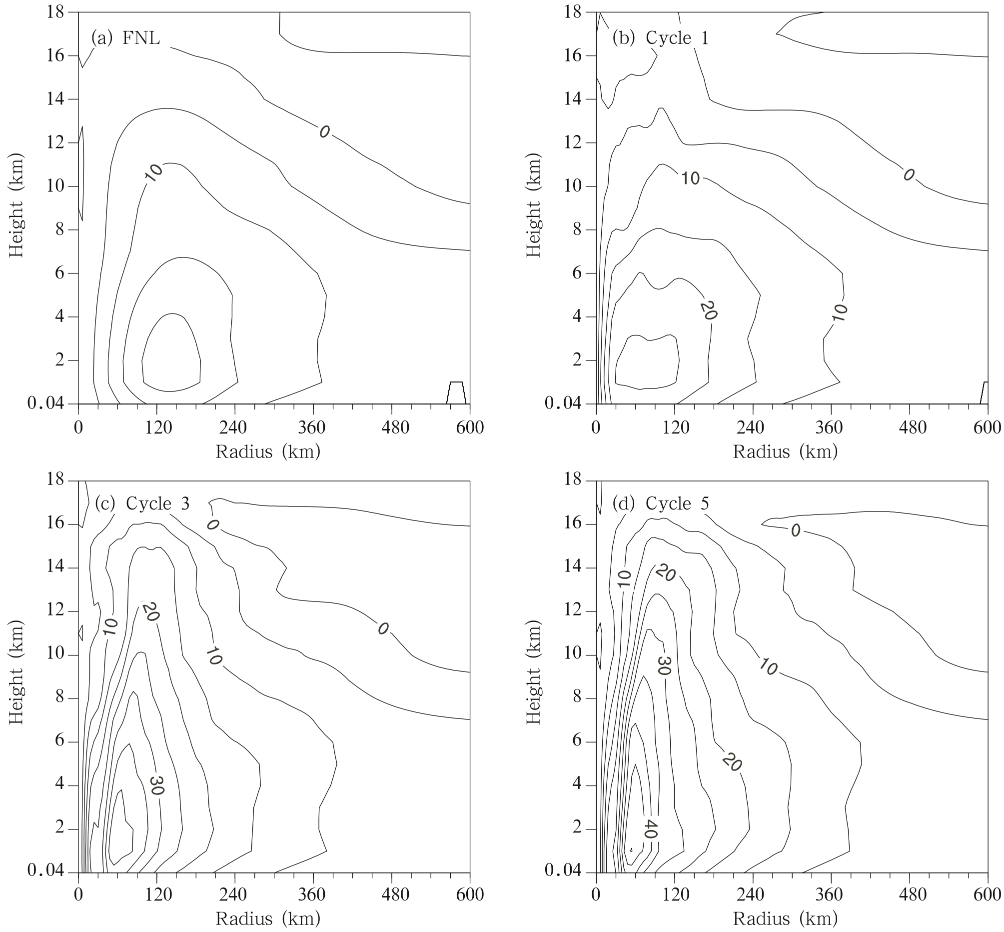

Fig. 6. Radial-vertical structure of the azimuthal mean tangential wind from (a) the NCEP FNL analysis and from the dynamical initialization after (b) 1 cycle run, (c) 3 cycle runs, and (d) 5 cycle runs for Typhoon Megi at 0000 UTC 15 October 2010.

the axisymmetric structure of the TC vortex in the FNL analysis is quite weak and has the radius of maximum wind (RMW) of 140 km in the lower troposphere (Fig. 6a). After 1 cycle run, the storm started to intensify and contracted in its inner core size (Fig. 6b). After 3 cycle runs, the storm continued intensifying with the RMW reduced to about 60 km with a deep cyclonic circulation (Fig. 6c). After 5 cycle runs, the storm further intensified and developed the structure typical of a mature TC with the RMW of about 50 km (Fig. 6d). Consistent with the primary circulation, the secondary circulation was also well developed through the cycle runs. As seen in Fig. 7, both the radial inflow in the boundary layer and the outflow in the upper troposphere are quite weak in the FNL analysis (Fig. 7a). After 3 and 5 cycle runs, both developed well (Figs. 7c and 7d), showing typical axisymmetric structure of a strong TC.

Since the DI scheme only spins up the axisymmetric component of the TC vortex, it is also our interest to look at the asymmetric structure of the storm. Figure 8 shows the zonal-vertical cross-sections of total wind speed and potential temperature across the TC center from the FNL analysis and from the DI after 1, 3, and 5 cycle runs, respectively. We can see that the TC vortex in the FNL analysis shows an east-west asymmetry in total wind speed with stronger winds to the east of the storm center (Fig. 8a). This asymmetry is maintained throughout the cycle runs (Figs. 8b–d). The above results indicate that the DI substantially improved the TC intensity and structure from the coarse-resolution FNL analysis.

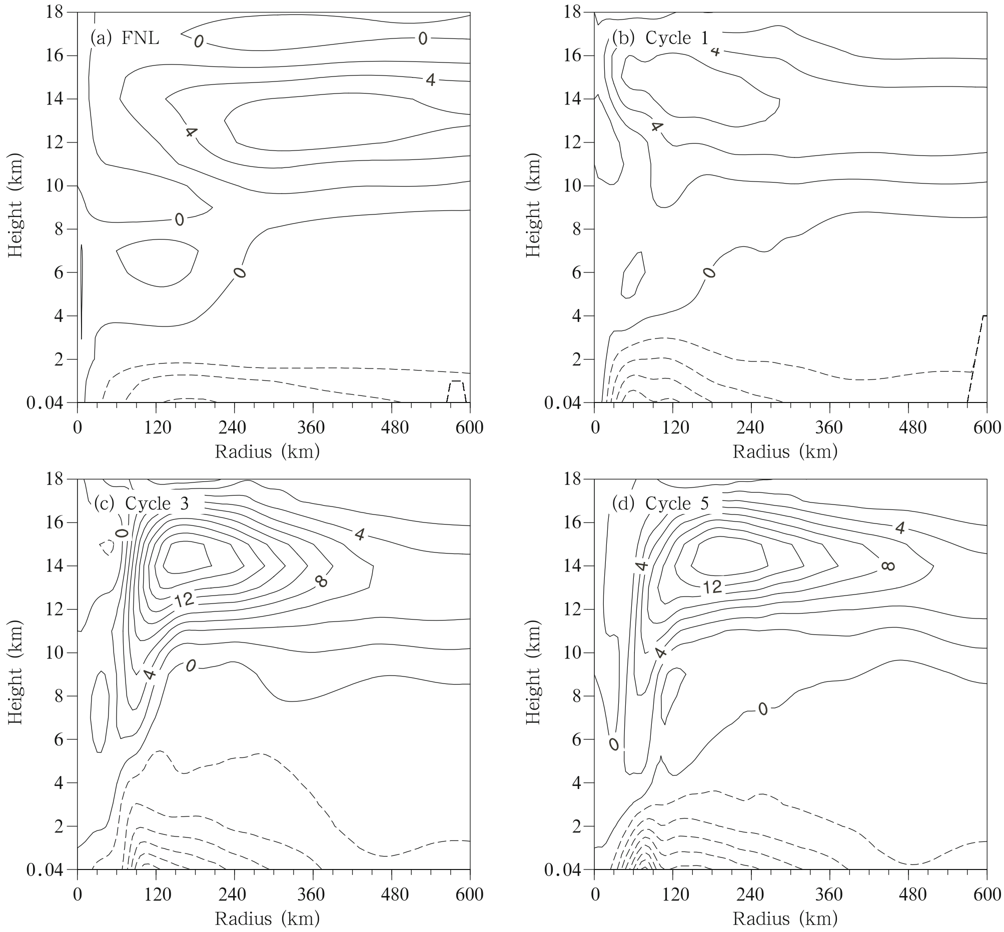

Fig. 7. As in Fig. 6, but for the azimuthal mean radial wind.

3.4 Experimental design

Four experiments were designed (Table 1) to demonstrate how the combined use of the DI scheme and the large-scale SN improves the subsequent simulation of Typhoon Megi. In the control (CTRL) experiment, both the DI scheme and the large-scale SN described in Sections 2 and 3.3 were used throughout the simulation. In the second experiment (SN_NDI), the DI scheme was not used while the large-scale SN was used throughout the simulation. In the third experiment (NSN_DI), the DI scheme was used while the large-scale SN was skipped in the simulation. In the last experiment (NSN_NDI), neither the DI scheme nor the large-scale SN was used in the simulation. The latter three simulations were designed as sensitivity experiments to demonstrate the advantages of the DI scheme and the large-scale SN in realistic simulation of a real TC.

Table 1. Summary of experiments performed in this study

Experiment	SN	DI
CTRL	Yes	Yes
SN_NDI	Yes	No
NSN_DI	No	Yes
NSN_NDI	No	No

In all experiments, the initial time was 0000 UTC 15 October 2010. As in the DI scheme, the initial and lateral boundary conditions and SST were interpolated from the FNL analysis data with a $1°\times1°$ resolution. The model was integrated for 168 h up to 0000 UTC 22 October for each experiment. Therefore, the simulation covered the initial RI period of Megi, the weakening during its landfall over the Luzon Island, and its re-intensification and sudden northward turning mo-

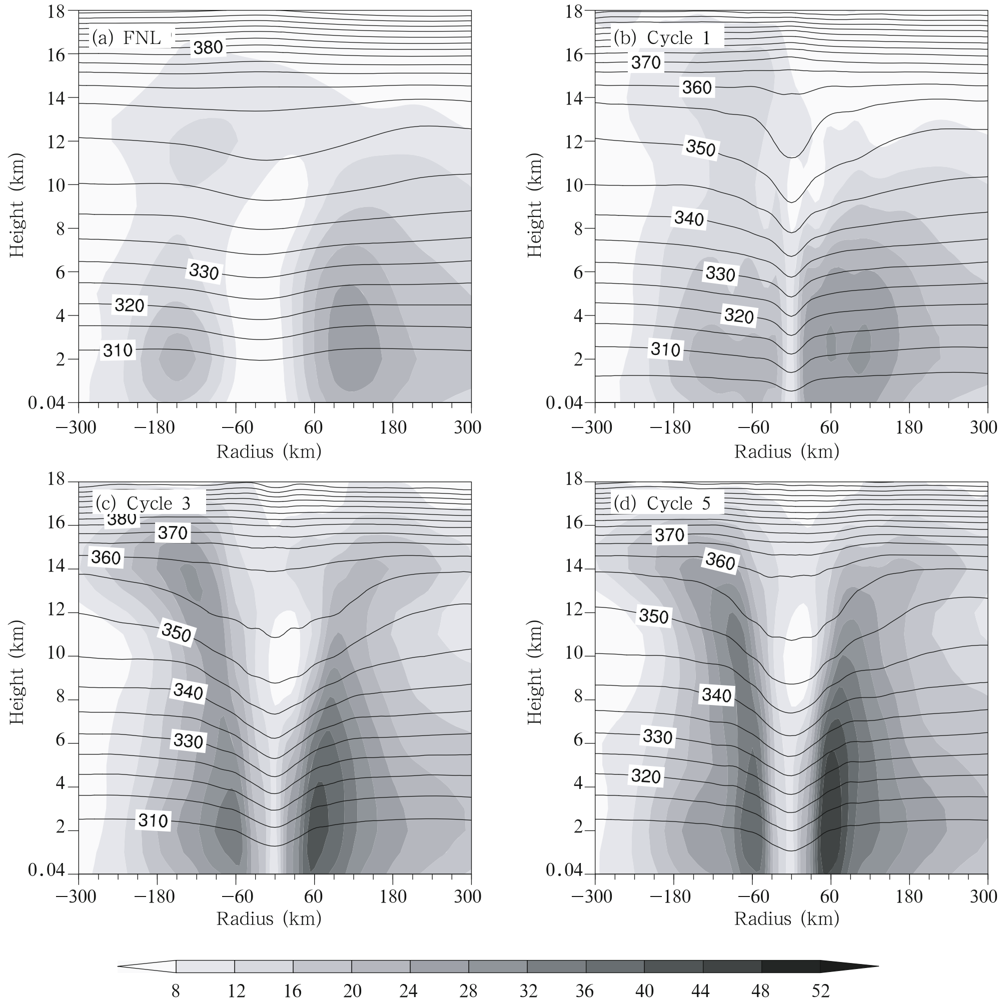

Fig. 8. Zonal-vertical cross-sections of the total horizontal wind speed (m s^{-1}; shaded) and potential temperature (K; contour) across the TC center from the FNL analysis (a) and from the DI after (b) 1 cycle run, (c) 3 cycle runs, and (d) 5 cycle runs valid at 0000 UTC 15 October 2010.

tion after it reentered the ocean over the SCS. In the next section, we will demonstrate that the use of the DI scheme and the large-scale SN considerably improves the simulated storm track, structure, and intensity changes.

4. Results

4.1 Storm track and intensity

Figure 9a shows the tracks of Typhoon Megi simulated in the four experiments listed in Table 1 together with the track from the JTWC best track data. All experiments simulated the west-northwestward movement in the first two days and the west-southwestward movement until the storm crossed the Luzon Island. The considerable difference among the four experiments occurred about one day after the storm crossed the Luzon Island and reentered the ocean over the SCS. In particular, the difference is large between simulations with and without the use of the large-scale SN. The tracks from the experiments with the SN (SN_DI and SN_NDI) are in good agreement with the JTWC best track data, especially from CTRL with the DI. The improved track forecast in these two experiments can be attributed to the improved large-scale circulation in the simulations as a result of the use of the large-scale SN (see Section 4.3 below). The track with the DI is closer to the best track than that without the DI, suggesting that the better representation of the initial TC structure from the DI also contributes to the improved track simulation. The track errors in the two experiments without the use of the SN are relatively large (Fig. 10a). The extremely large track errors are related to the substantially delayed northward turning after the storm entered the SCS, in particular for the simulation without the DI (Fig. 10a). Only the CTRL experiment with both the DI and large-scale SN captured the timing and location of the observed northward turning motion over the SCS realistically (Fig. 9).

The simulated storm intensity also shows sensitivity to both the DI and the SN (right panels in Fig. 9). Overall, all experiments simulated well the intensity change in terms of the central SLP and the maximum

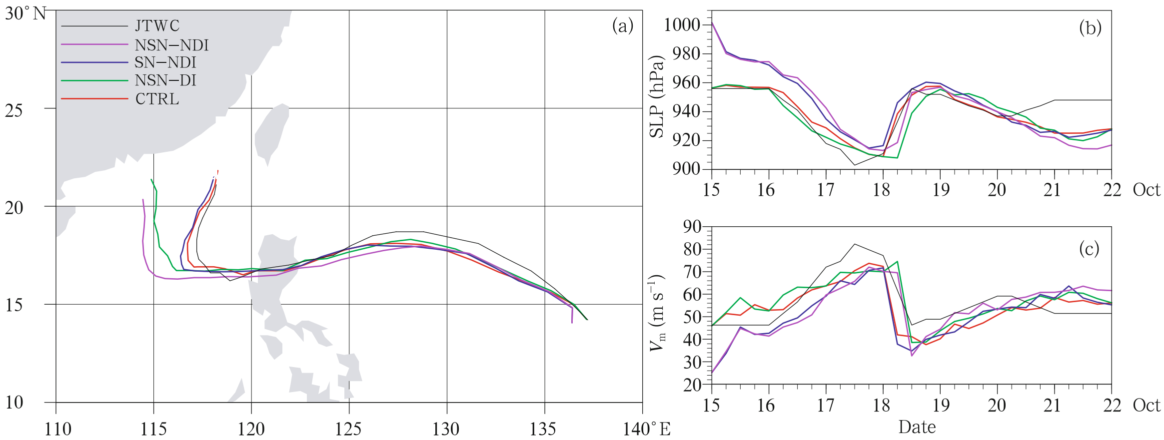

Fig. 9. (a) Track of Typhoon Megi, and the time series of (b) central sea level pressure (hPa) and (c) maximum sustained 10-m wind speed (m s^{-1}) from 0000 UTC 15 to 0000 UTC 22 October 2010 from the JTWC best track data (black) and from the four experiments listed in Table 1.

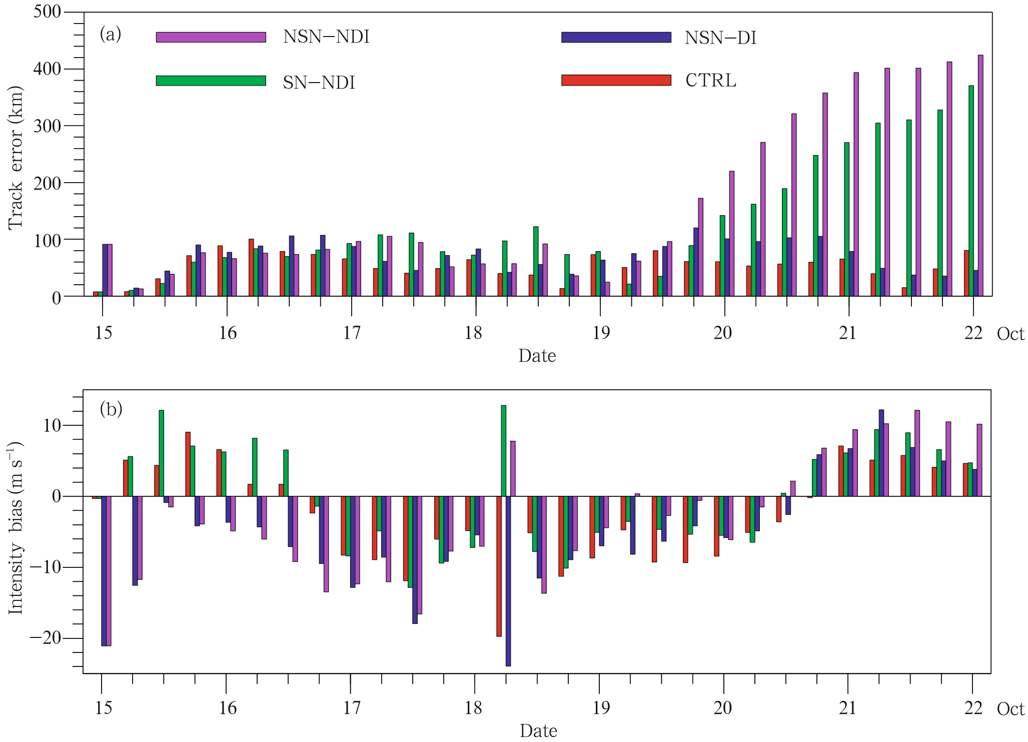

Fig. 10. Simulated TC (a) track errors (km) and (b) intensity biases (m s^{-1}) in the four experiments listed in Table 1.

sustained surface wind speed. Namely, all experiments simulated the rapid intensification of the observed storm before it made landfall over the Luzon Island, the rapid weakening after landfall across the Luzon Island, and the re-intensification of the storm after it reentered the ocean over the SCS. Nevertheless, the simulations with the DI in general produced the storm intensity in better agreement with the best track data than those without the DI (Fig. 10b). In particular, the simulations without the DI show large negative intensity biases in the first 2–3 days due to the weak intensity of the initial TC vortex in the FNL analysis. However, all experiments failed to reproduce the slow weakening and thus overestimated the storm intensity after 0600 UTC 20 October when the storm moved north-northeastward over the SCS. This was partially due to the ignorance of the negative ocean feedback because the daily mean SST was used in all simulations. Note that although large differences occurred between the experiments with and without the DI, the intensity bias show similar tendencies (Fig. 10b), indicating that the difference in storm track did not contribute significantly to the intensity bias in the Megi case. The large intensity bias around 0600 UTC 18 October in both CTRL and SN_NDI is related to slightly earlier landfall of the storm in the simulations than in the observation. Note also that the intensity biases are relatively large compared to the track errors even though the DI scheme was used, indicating that it is still a challenge to realistically simulate TC intensity by high-resolution numerical models.

The above results show that the simulated storm track can be largely improved with the use of the large-scale SN, while the simulated storm intensity can be improved with the use of the DI scheme, at least for the first 6–12 h. Overall, the CTRL simulation with both the DI and the large-scale SN reproduced both the track and intensity changes better than any of the other three experiments. This suggests that the approach described in Section 2 can be used to achieve improved simulations of the track and intensity of real TC cases if a good global analysis is available and used to drive a high-resolution regional atmospheric model.

4.2 Storm structure change

A detailed verification of the three-dimensional structure of the simulated storm is impossible since there are few observations available over the open ocean. Here we roughly compare the cloud/precipitation structure based on the cloud/precipitation features from satellite observations, such as the MIMIC-IR (Morphed Integrated Microwave Imagery at CIMSS, with infrared) images as shown in Fig. 11. Since the brightness temperature is highly correlated with deep convection and heavy precipitation, it is qualitatively comparable to the model simulated radar reflectivity near the surface, which reflects surface precipitation.

At 2000 UTC 15 October, just before the RI started, the storm displayed considerable convective asymmetric structure in the eyewall, with enhanced and wide convective area in the northeast quadrant and a much narrower eyewall to the south (Fig. 11a). An inner and an outer spiral rainbands extended outward from the eyewall to the southeast. The overall cloud/precipitation structure was simulated reasonably well in the two experiments with the DI (CTRL and NSN_DI) though the simulation without the SN (NSN_DI) produced convection too strong in the southern eyewall (Figs. 12a and 12b). In sharp contrast, the two experiments without the DI simulated partial eyewall structure with eyewall convection to the south almost missing (Figs. 12c and 12d). Since the results shown in Figs. 11a–d are only after 20 h of model integration, it is suggested that the DI of the initial TC vortex significantly improved the storm structure in the early model simulation.

By 2300 UTC 17 October, at the time just before the storm made landfall over the Luzon Island, the storm developed double eyewall structure and increased in its size with active outer spiral rainbands to the northeast and over the Luzon Island (Fig. 11b). The overall structure was simulated reasonably well in all experiments except for the failure of the double eyewall structure at the given time in the simulation and the difference in the simulated storm position

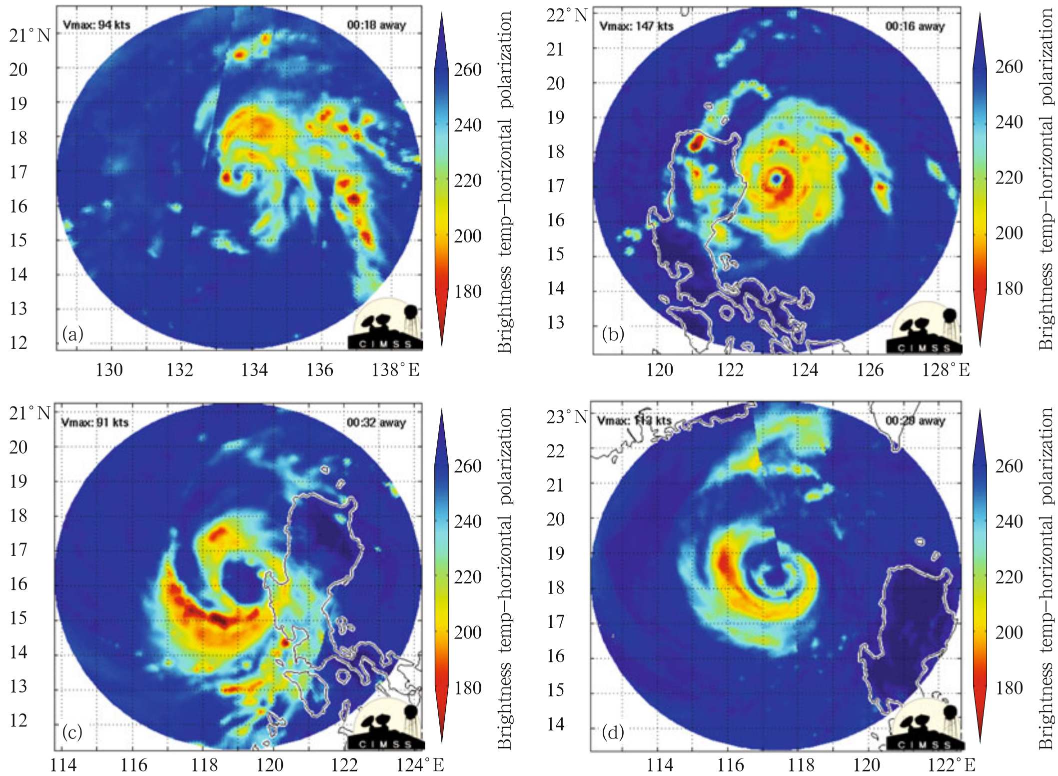

Fig. 11. The MIMIC-IR images at (a) 2000 UTC 15, (b) 2300 UTC 17, (c) 0100 UTC 19, and (d) 0900 UTC 20 October. The labels at top left of each panel denote the NHC (National Hurricane Center)-reported maximum sustained winds, and those at top right of each panel denote the temporal separation from the microwave overpass nearest in time.

(Figs. 12e–h). Despite the failure in simulating the double eyewall structure just before the landfall of the storm, all experiments simulated a double eyewall structure after the storm made landfall and moved over the Luzon Island as a result of the rapid contraction and then the weakening of the original eyewall and the sustaining of the strong outer quasi-symmetric rainbands (figure omitted). Note that the difference between the experiments with and without the DI becomes insignificant in Figs. 12e–h, suggesting that the DI affects the simulated storm structure mainly in the first day before the storm developed well in the Megi case.

Megi exhibited a drastic eyewall structure change after it crossed the Luzon Island and entered the SCS (Fig. 3). The original eyewall disappeared when the storm moved over the Luzon Island. After the storm entered the SCS, it formed a new large eyewall as a result of the axisymmetrization of the outer spiral rainband. This is because the outer circulation/rainband remained strong when the storm moved across the Luzon Island even though its inner core intensity substantially weakened (Figs. 3 and 11c). Similar features have been previously described for storms that crossed the Luzon Island based on both observations and numerical simulations (Wu et al., 2003, 2009; Chou et al., 2011). At the time given in Fig. 11c, the new eyewall was at its formation stage with strong convection to the northwest, a strong and wide convective spiral rainband extending from the new eyewall to the southwest, and some loosely organized convective activities to the southeast. The overall structure, including the asymmetric structure, was simulated reasonably well in all experiments (Figs. 12i–l). The phase of the convective asymmetries was better simulated in the two experiments with the DI (Figs. 12i and 12j). The storm simulated in NSN_NDI showed stronger eyewall convection and was more axisymmetric than the storm simulated in any other experiments (Fig. 12l). The storm in SN_NDI developed strong convection to

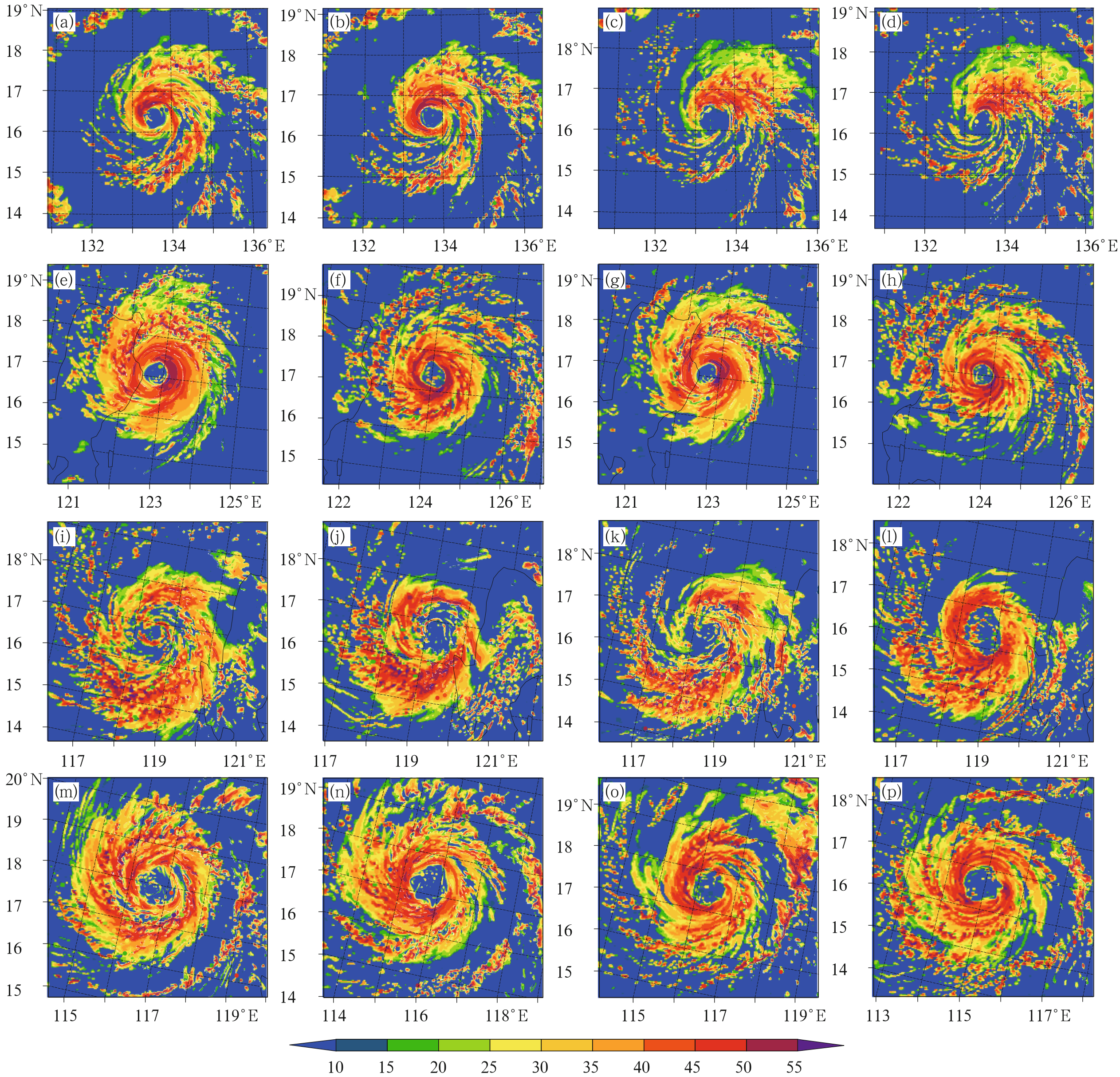

Fig. 12. The model simulated radar reflectivity at $\sigma = 0.9215$ at (a–d) 2000 UTC 15, (e–h) 2300 UTC 17, (i–l) 0100 UTC 19, and (m–p) 0900 UTC 20 October 2010 from experiments (a, e, i, m) CTRL, (b, f, j, n) NSN_DI, (c, g, k, o) SN_NDI, and (d, h, l, p) NSN_NDI.

the northeast in the new eyewall (Fig. 12k) instead of the northwest in the observation (Fig. 11c).

Megi developed a double eyewall structure again as it re-intensified over the SCS (Fig. 11d). The development of the double eyewall structure was partly responsible for the observed weakening of the storm after 0600 UTC 20 October. None of the experiments simulated the formation of the double eyewall structure as observed (Figs. 12m–p). Note that the CTL experiment produced an apparent double eyewall structure but not as typical as that observed (Fig. 12m). As a result, all experiments failed to simulate the weakening of Megi after 20 October. Nevertheless, overall, both the DI and the large-scale SN contributed to the improved simulation of the storm structure evolution although some discrepancies exist. The results from CTRL could thus be analyzed to understand the physical mechanisms responsible for the structure change when Megi crossed the Luzon Island as well as the possible terrain and landmass effects of the Luzon Island in a future study.

4.3 Effect of spectral nudging

We have already shown above that the large-scale SN considerably improved the simulation of Typhoon Megi, in particular its track. This is due to the fact that the large-scale SN effectively preserved the large-scale environmental flow. This can be measured by the root mean square error (RMSE) for any given variable of the large-scale component in the model simulation from the FNL analysis (namely, the driving field). Figure 13 shows the time series of the RMSEs for both zonal and meridional winds at 500 hPa in the four experiments listed in Table 1. The RMSEs for the experiments with and without the DI are quite close to each other, indicating that the DI of the TC vortex has little effect on the large-scale environmental field. In sharp contrast, the large difference occurs between the experiments with and without the use of the large-scale SN. For example, throughout the 7-day simulation, the RMSEs for both zonal and meridional winds are generally less than 0.6–0.7 m s^{-1} in the two experiments with the SN while they increased with time almost linearly in the first 2–3 days and then remained as large as about 2.2–2.5 m s^{-1}, nearly 3–3.5 times larger than those with the large-scale SN. Note that the track errors remained small in the first 5-day simulation even without the use of the large-scale SN (Fig. 10a). This is mainly because errors in the large-scale wind field appeared in the midlatitude where the error grows much faster than that in the tropics while the storm was located in the deep tropics. Nevertheless, the large errors in the large-scale wind field eventually led to large errors in the simulated storm track in the last two days (Fig. 10a). The results therefore demonstrate that the use of the large-scale SN effectively preserves the environmental flow and thus improves the simulation of storm motion.

Figure 14 shows the large-scale component of geopotential height at 500 hPa after 3-, 5-, and 7-day simulation in CTRL and NSN_DI experiments, respectively. The simulated large-scale geopotential height field in the experiment with the large-scale SN (CTRL simulation) shows little deviation from that in the FNL analysis throughout the simulation (Figs. 14a, 14c, and 14e). In the experiment without the large-scale SN (NSN_DI), the simulated large-scale component of geopotential height field shows considerable deviation from the FNL analysis (Figs. 14b, 14d, and 14f). The deviation increased with time in the simulation without the SN. After the storm crossed the Luzon Island, the WNP subtropical high weakened and retreated eastward in the FNL analysis (Fig. 14). The southerly wind west of the subtropical high steered the storm northward around 20 October (Fig. 9). This was well simulated in the CTRL experiment with the SN. In the experiment without the SN, the simulated subtropical high is stronger than the observed, which led to a slightly faster movement and considerably delayed the northward turning of the simulated storm (Fig. 9). By the end of the 7-day simulation, considerable deviation in the large-scale geopotential height field is obvious. It is featured with the strengthening of a ridge northeast of the simulated storm, leading to a westward track error in the expe-

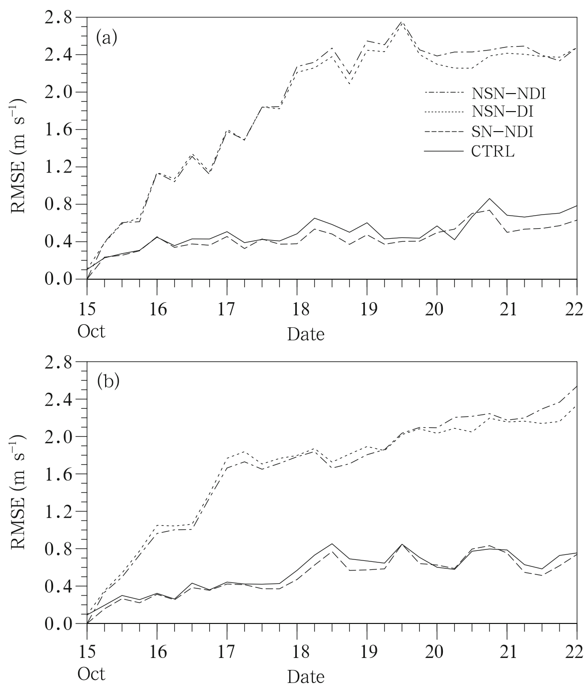

Fig. 13. Time evolution the RMSEs of the large-scale (a) zonal and (b) meridional winds at 500 hPa in the four experiments listed in Table 1.

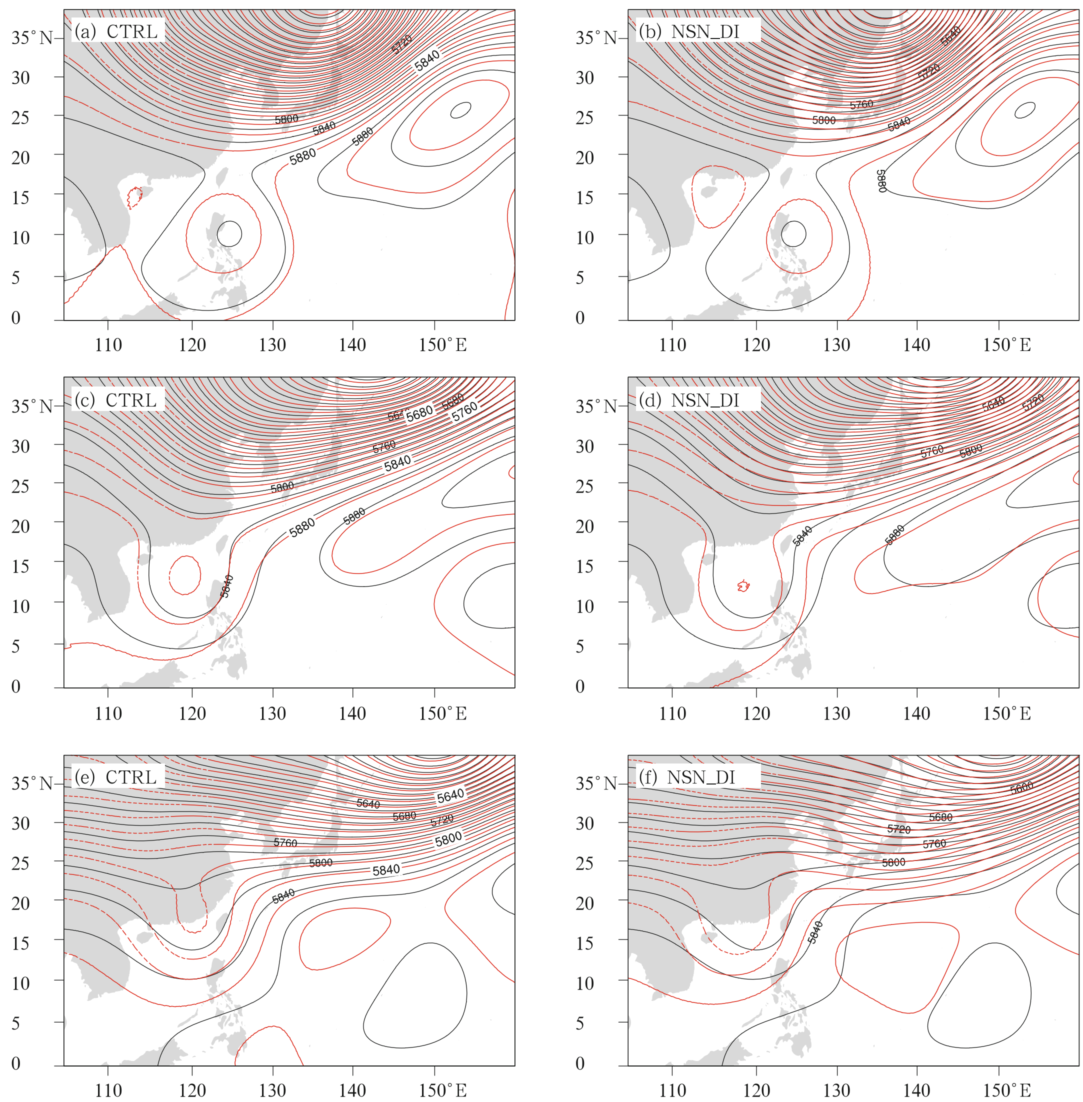

Fig. 14. Filtered geopotential height fields at 500 hPa at 0000 UTC (a, b) 18, (c, d) 20, and (e, f) 22 October 2010 from the FNL in black and from the (a, c, e) control experiment and (b, d, f) NSN_DI in red.

riments without the large-scale SN.

The results above demonstrated that the use of the SN reduced the model bias in the large-scale environmental flow and thus improved the simulated storm track. Without the SN, the model bias in the simulated large-scale environmental flow increased with time and led to considerable bias in the simulated storm track. As a result, if the focus of a study is not on how the TC affects the large-scale environmental flow, the large-scale SN is an attractive approach to achieving the realistic simulations of a real TC in a high-resolution regional atmospheric model if a good global analysis is available and used to drive the regional model.

5. Conclusions

In this study, we have presented a new approach, which combines a DI scheme with 3-h cycle runs and the large-scale SN, to achieving improved simulations of a real TC, including its track, structure, and intensity changes, using the advanced WRF model. The DI scheme effectively provides realistic high-resolution initial conditions for the targeted TC. In this DI scheme, the axisymmetric component of the TC vortex in the coarse-resolution global analysis is replaced by the more realistic and dynamically-constrained axisymmetric TC vortex after each 3-h cycle run. The asymmetric component is implicitly assumed to be resolved well in the global analysis field and is thus kept unchanged at the initial time of the cycle runs. The cycle run is terminated once the intensity of the model TC is comparable to that observed. The DI scheme has been shown to be able to improve not only the simulated TC intensity but also the simulated TC structure. To reduce the bias in the simulated large-scale environmental flow, which controls the TC motion, the large-scale SN approach is used to the wind field in the outermost model domain. The SN is applied not only during the cycle runs but also throughout the subsequent model simulation.

The effectiveness of the proposed approach has been demonstrated with a case study of Typhoon Megi (2010) using the ARW-WRF model. The control experiment with the proposed approach realistically reproduced many aspects of Typhoon Megi in a week-long simulation. The model simulated quite well the storm track, and structure and intensity changes. In particular, the model captured not only the rapid intensification and the size increase before Megi made landfall over the Luzon Island, but also its drastic structure changes when Megi crossed the Luzon Island in the northern Philippines. The control simulation also reproduced the re-intensification and the formation of the new large eyewall after Megi entered the SCS. The results from several sensitivity experiments show that the use of the large-scale SN contributed greatly to the improved track simulation, in particular for the simulation after three days, while the use of the DI scheme mainly improved the storm intensity and structure in the first 2–3-day simulation. Overall, the results demonstrate that the combined use of the DI and the SN is quite effective and ideal for achieving improved simulation for the process studies focusing on TC inner-core dynamics, and structure and intensity changes. Our detailed studies to understand the rapid intensification, size change, and intensity and structure changes in Typhoon Megi are underway and the results will be reported separately.

Because the main purpose of this paper is to introduce the new approach, its effectiveness has been examined by one simulation. However, results from some extra experiments with different initial times are also promising (figure omitted). Nevertheless, more case studies are required to demonstrate the robustness and applicability of the proposed approach in future studies. In addition, the DI scheme can be combined with a four-dimensional data assimilation system during the cycle runs to further improve the initial TC structure. Note that although the approach has been developed based on the ARW-WRF model, it can be easily transferred to any other high-resolution models since it was constructed as an individual module.

Finally, it should be mentioned that the approach proposed in this study has some limitations. Firstly, the approach is better applied to well-defined TC systems since if the system is too weak, the axisymmetric component may not be well determined. Secondly, the cycle runs only spin up the axisymmetric component of a TC. As a result, if a storm has significant asymmetric structure in particular in the inner core region, the approach will not work properly. Thirdly, since the azimuthal mean is performed to construct the axisymmetric TC vortex after each cycle run, once the TC is approaching any topography, the approach will have errors since extrapolations need to be used. As a result, when the targeted TC is too close to topography, the approach is not recommended. In that case, the earlier initial time can be considered for the simulation. This may not be a barrier for the application of the proposed approach since it is proposed to improve numerical simulations not prediction. Nevertheless, it will be a good topic for a future study to extend the current work to include the asymmetric structure, which is beyond the scope of this work.

Acknowledgments. The authors are grateful to two anonymous reviewers for their helpful comments.

REFERENCES

Bender, M. A., I. Ginis, and Y. Kurihara, 1993: Numerical simulations of tropical cyclone-ocean interaction with a high-resolution coupled model. *J. Geophys. Res.*, **98**(D12), 23245–23263.

Braun, S. A., 2002: A cloud-resolving simulation of Hurricane Bob (1991): Storm structure and eyewall buoyancy. *Mon. Wea. Rev.*, **130**(6), 1573–1592.

——, 2006: High-resolution simulation of Hurricane Bonnie (1998). Part II: Water budget. *J. Atmos. Sci.*, **63**(1), 43–64.

——, and W. K. Tao, 2000: Sensitivity of high-resolution simulations of Hurricane Bob (1991) to planetary boundary layer parameterizations. *Mon. Wea. Rev.*, **128**(12), 3941–3961.

——, M. T. Montgomery, and Z. -X. Pu, 2006: High-resolution simulation of Hurricane Bonnie (1998). Part I: The organization of eyewall vertical motion. *J. Atmos. Sci.*, **63**(1), 19–42.

Cha, D. -H., C. -S. Jin, D. -K. Lee, et al., 2011: Impact of intermittent spectral nudging on regional climate simulation using Weather Research and Forecasting model. *J. Geophys. Res.*, **116**, D10103, doi: 10.1029/2010JD015069.

——, and Y. Q. Wang, 2013: A dynamical initialization scheme for real-time forecasts of tropical cyclones using the WRF model. *Mon. Wea. Rev.*, **141**(3), 964–986.

Chou, K. -H., C. -C. Wu, Y. Wang, et al., 2011: Eyewall evolution of typhoons crossing the Philippines and Taiwan: An observational study. *Terr. Atmos. Ocean. Sci.*, **22**(6), 535–548.

Cram, T. A., J. Persing, M. T. Montgomery, et al., 2007: A Lagrangian trajectory view on transport and mixing processes between the eye, eyewall, and environment using a high-resolution simulation of Hurricane Bonnie (1998). *J. Atmos. Sci.*, **64**(6), 1835–1856.

Davis, C. A., and L. F. Bosart, 2001: Numerical simulations of the genesis of Hurricane Diana (1984). Part I: Control simulation. *Mon. Wea. Rev.*, **129**(8), 1859–1881.

——, and S. Low-Nam, 2001: The NCAR-AFWA Tropical Cyclone Bogussing Scheme. Air Force Weather Agency (AFWA) Rep., 12 pp. [Available online at http://www.mmm.ucar.edu/mm5/mm5v3/tc-bogus.html.]

——, and L. F. Bosart, 2002: Numerical simulations of the genesis of Hurricane Diana (1984). Part II: Sensitivity of track and intensity prediction. *Mon. Wea. Rev.*, **130**(5), 1100–1124.

——, W. Wang, S. S. Chen, et al., 2008: Prediction of landfalling hurricanes with the advanced hurricane WRF model. *Mon. Wea. Rev.*, **136**(6), 1990–2005.

Dudhia, J., 1989: Numerical study of convection observed during the Winter Monsoon Experiment using a mesoscale two-dimensional model. *J. Atmos. Sci.*, **46**(20), 3077–3107.

Ek, M. B., K. E. Mitchell, Y. Lin, et al., 2003: Implementation of Noah land surface model advances in the National Centers for Environmental Prediction operational mesoscale Eta model. *J. Geophys. Res.*, **108**, 8851, doi: 10.1029/2002JD003296.

Feser, F., and H. von Storch, 2008: A dynamical downscaling case study for typhoons in Southeast Asia using a regional climate model. *Mon. Wea. Rev.*, **136**(5), 1806–1815.

Goerss, J. S., and R. A. Jeffries, 1994: Assimilation of synthetic tropical cyclone observations into the Navy Operational Global Atmospheric Prediction System. *Wea. Forecasting*, **9**(4), 557–576.

Hendricks, E. A., M. S. Peng, X. -Y. Ge, et al., 2011: Performance of a dynamic initialization scheme in the Coupled Ocean-Atmosphere Mesoscale Prediction System for Tropical Cyclones (COAMPS-TC). *Wea. Forecasting*, **26**(5), 650–663.

Hogsett, W., and D. -L. Zhang, 2009: Numerical simulation of Hurricane Bonnie (1998). Part III: Energetics. *J. Atmos. Sci.*, **66**(9), 2678–2696.

——, and ——, 2010: Genesis of Typhoon Chanchu (2006) from a westerly wind burst associated with the MJO. Part I: Evolution of a vertically tilted precursor vortex. *J. Atmos. Sci.*, **67**(12), 3774–3792.

——, and ——, 2011: Genesis of Typhoon Chanchu (2006) from a westerly wind burst associated with the MJO. Part II: Roles of deep convection in tropical transition. *J. Atmos. Sci.*, **68**(6), 1377–1396.

Holland, G. J., 1983: Tropical cyclone motion: Environmental interaction plus a beta effect. *J. Atmos. Sci.*, **40**(2), 328–342.

Hong, S. -Y., and J. -O. J. Lim, 2006: The WRF single-moment 6-class microphysics scheme (WSM6). *J. Korean Meteor. Soc.*, **42**(2), 129–151.

Kain, J. S., 2004: The Kain-Fritsch convective parameterization: An update. *J. Appl. Meteor.*, **43**(1), 170–181.

——, and J. M. Fritsch, 1990: A one-dimensional entraining/detraining plume model and its application in convective parameterization. *J. Atmos. Sci.*, **47**(23), 2784–2802.

——, and J. M. Fritsch, 1993: Convective parameterization for mesoscale models: The Kain-Fritsch scheme. *The Representation of Cumulus Convection in Numerical Models*, Meteor. Monogr. No. 24, Amer. Meteor. Soc., 165–170.

Kida, H., T. Koide, H. Sasaki, et al., 1991: A new approach for coupling a limited area model to a GCM for regional climate simulations. *J. Meteor. Soc. Japan*, **69**, 723–728.

Kurihara, Y., M. A. Bender, and R. J. Ross, 1993: An initialization scheme of hurricane models by vortex specification. *Mon. Wea. Rev.*, **121**(7), 2030–2045.

——, ——, R. E. Tuleya, et al., 1995: Improvements in the GFDL Hurricane Prediction System. *Mon. Wea. Rev.*, **123**(9), 2791–2801.

Kwon, I. -H., and H. -B. Cheong, 2010: Tropical cyclone initialization with a spherical high-order filter and an idealized three-dimensional bogus vortex. *Mon. Wea. Rev.*, **138**(4), 1344–1367.

Leslie, L. M., and G. J. Holland, 1995: On the bogussing of tropical cyclones in numerical models: A comparison of vortex profiles. *Meteor. Atmos. Phys.*, **56**(1–2), 101–110.

Li, X. -L., and Z. -X. Pu, 2008: Sensitivity of numerical simulation of early rapid intensification of Hurricane Emily (2005) to cloud microphysical and planetary boundary layer parameterizations. *Mon. Wea. Rev.*, **136**(12), 4819–4838.

Liu, B., and L. Xie, 2012: A scale-selective data assimilation approach to improving tropical cyclone track and intensity forecasts in a limited-area model: A case study of Hurricane Felix (2007). *Wea. Forecasting*, **27**(1), 124–140.

Liu, Y. B., D. -L. Zhang, and M. K. Yau, 1997: A multiscale numerical study of Hurricane Andrew (1992). Part I: Explicit simulation and verification. *Mon. Wea. Rev.*, **125**(12), 3073–3093.

——, ——, and ——, 1999: A multiscale numerical study of Hurricane Andrew (1992). Part II: Kinematics and inner-core structures. *Mon. Wea. Rev.*, **127**(11), 2597–2616.

Ma, S. -H., A. -X. Qu, and Y. Wang, 2007: The performance of the new tropical cyclone track prediction system of the China National Meteorological Center. *Meteor. Atmos. Phys.*, **97**(1–4), 29–39.

Miguez-Macho, G., G. L. Stenchikov, and A. Robock, 2005: Regional climate simulations over North America: Interaction of local processes with improved large-scale flow. *J. Climate*, **18**(8), 1227–1246.

Mlawer, E. J., S. J. Taubman, P. D. Brown, et al., 1997: Radiative transfer for inhomogeneous atmospheres: RRTM, a validated correlated-k model for the longwave. *J. Geophys. Res.*, **102**(D14), 16663–16682.

Moon, I.- J., I. Ginis, T. Hara, et al., 2007: A physics-based parameterization of air-sea momentum flux at high wind speeds and its impact on hurricane intensity predictions. *Mon. Wea. Rev.*, **135**(8), 2869–2878.

Musgrave, K. D., C. A. Davis, and M. T. Montgomery, 2008: Numerical simulations of the formation of Hurricane Gabrielle (2001). *Mon. Wea. Rev.*, **136**(8), 3151–3167.

Nakanishi, M., and H. Niino, 2004: An improved Mellor-Yamada Level-3 model with condensation physics: Its design and verification. *Boundary-Layer Meteor.*, **112**(1), 1–31.

Peng, M. S., B. -F. Jeng, and C. -P. Chang, 1993: Forecast of typhoon motion in the vicinity of Taiwan during 1989–90 using a dynamical model. *Wea. Forecasting*, **8**(3), 309–325.

Pu, Z. -X., and S. A. Braun, 2001: Evaluation of bogus vortex techniques with four-dimensional variational data assimilation. *Mon. Wea. Rev.*, **129**(8), 2023–2039.

Riette, S., and D. Caya, 2002: Sensitivity of short simulations to the various parameters in the new CRCM spectral nudging. Research Activities in Atmospheric and Oceanic Modelling, Ritchie H., Ed., WMO/TD-No 1105, Report No. 32, 7.39–7.40.

Rogers, M. L. Black, S. S. Chen, et al., 2007: An evaluation of microphysics fields from mesoscale model simulations of tropical cyclones. Part I: Comparisons with observations. *J. Atmos. Sci.*, **64**(6), 1811–1834.

Rogers, R., 2010: Convective-scale structure and evolution during a high-resolution simulation of tropical cyclone rapid intensification. *J. Atmos. Sci.*, **67**(1), 44–70.

Tallapragada, V., Y. C. Kwon, Q. Liu, et al., 2012: Operational implementation of high-resolution triply-nested HWRF at NCEP/EMC—A major step towards addressing intensity forecast problem. The 30th Conference on Hurricanes and Tropical Meteorology, Amer. Meteor. Soc., 15–20 April 2012, Ponte Vedra Beach, Florida.

Ueno, M., 1989: Operational bogussing and numerical prediction of typhoon in JMA. JMA/NPD Tech. Rep., 28, 48 pp.

van Nguyen, H., and Y. -L. Chen, 2011: High-resolution initialization and simulations of Typhoon Morakot (2009). *Mon. Wea. Rev.*, **139**(5), 1463–1491.

von Storch, H., H. Langenberg, and F. Feser, 2000: A spectral nudging technique for dynamical downscaling purposes. *Mon. Wea. Rev.*, **128**(10), 3664–3673.

Wang, Y. Q., 1998: On the bogussing of tropical cyclones in numerical models: The influence of vertical structure. *Meteor. Atmos. Phys.*, **65**(3–4), 153–170.

—–, 2001: An explicit simulation of tropical cyclones with a triply nested movable mesh primitive equation model: TCM3. Part I: Model description and control experiment. *Mon. Wea. Rev.*, **129**(6), 1370–1394.

Wu, C. -C., K. -H. Chou, H. -J. Cheng, et al., 2003: Eyewall contraction, breakdown and reformation in a landfalling typhoon. *Geophys. Res. Lett.*, **30**(17), 1887, doi: 10.1029/2003GL017653.

—–, H. J. Cheng, Y. Q. Wang, et al., 2009: A numerical investigation of the eyewall evolution of a landfalling typhoon. *Mon. Wea. Rev.*, **137**(1), 21–40.

Yang, M. -J., D. -L. Zhang, and H. -L. Huang, 2008: A modeling study of Typhoon Nari (2001) at landfall. Part I: Topographic effects. *J. Atmos. Sci.*, **65**(10), 3095–3115.

—–, —–, X. -D. Tang, et al., 2011: A modeling study of Typhoon Nari (2001) at landfall. Part II: Structural changes and terrain-induced asymmetries. *J. Geophys. Res.*, **116**, D09112, doi: 10.1029/2010JD015445.

Yau, M. K., Y. B. Liu, D. -L. Zhang, et al., 2004: A multiscale numerical study of Hurricane Andrew (1992). Part VI: Small-scale inner-core structures and wind streaks. *Mon. Wea. Rev.*, **132**(6), 1410–1433.

Zhang, D. -L., Y. B. Liu, and M. K. Yau, 2000: A multiscale numerical study of Hurricane Andrew (1992). Part III: Dynamically-induced vertical motion. *Mon. Wea. Rev.*, **128**(11), 3772–3788.

—–, —–, and —–, 2001: A multiscale numerical study of Hurricane Andrew (1992). Part IV: Unbalanced flows. *Mon. Wea. Rev.*, **129**(1), 92–107.

—–, —–, and —–, 2002: A multiscale numerical study of Hurricane Andrew (1992). Part V: Inner-core thermodynamics. *Mon. Wea. Rev.*, **130**(11), 2745–2763.

—–, L. Tian, and M. J. Yang, 2011: Genesis of Typhoon Nari (2001) from a mesoscale convective system. *J. Geophys. Res.*, **116**, D23104, doi: 10.1029/2011JD016640.

Zhang, Q. -H., S. -J. Chen, Y. -H. Kuo, et al., 2005: Numerical study of a typhoon with a large eye: Model simulation and verification. *Mon. Wea. Rev.*, **133**(4), 725–742.

Zhang, X. Y., Q. N. Xiao, and P. J. Fitzpatrick, 2007: The impact of multisatellite data on the initialization and simulation of Hurricane Lili's (2002) rapid weakening phase. *Mon. Wea. Rev.*, **135**(2), 526–548.

Zhu, T., D. -L. Zhang, and F. Z. Weng, 2004: Numerical simulation of Hurricane Bonnie (1998). Part I: Eyewall evolution and intensity changes. *Mon. Wea. Rev.*, **132**(1), 225–241.

—–, and —–, 2006: Numerical simulation of Hurricane Bonnie (1998). Part II: Sensitivity to varying cloud microphysical processes. *J. Atmos. Sci.*, **63**(1), 109–126.

Zou, X. L., and Q. N. Xiao, 2000: Studies on the initialization and simulation of a mature hurricane using a variational bogus data assimilation scheme. *J. Atmos. Sci.*, **57**(6), 836–860.